Composites Science and Technology 218 (2022) 109186

Contents lists available at ScienceDirect

Composites Science and Technology

journal homepage: www.elsevier.com/locate/compscitech

Prediction of stiffness degradation based on machine learning: Axial elastic modulus of $[0_m/90_n]_s$ composite laminates

Mingqing Yuan [a], Haitao Zhao [a,*], Yuehan Xie [b], Hantao Ren [b], Li Tian [a], Zhuoxin Wang [a], Boming Zhang [c], Ji'an Chen [a,**]

[a] School of Aeronautics and Astronautics, Shanghai Jiao Tong University, Shanghai, 200240, China
[b] Composites Centre, Commercial Aircraft Corporation of China Ltd, Shanghai, 201210, China
[c] School of Materials Science and Engineering, Beihang University, Beijing, 100191, China

ARTICLE INFO

Keywords:
Matrix cracking
Stiffness degradation
Machine learning
Cross-ply laminates
Kernel ridge regression

ABSTRACT

This paper, for the first time, proposed an axial elastic modulus degradation prediction method of $[0_m/90_n]_s$ cross-ply laminates using a machine learning (ML) model. The data set of the ML model is established based on the published experiments and a small amount of finite element analysis (FEA) results. The effect of data size on the accuracy of ML prediction is also discussed. The proposed ML model focuses on the process of translating a mechanical problem of damage into a non-linear regression problem of ML, and the mapping between the input and output data, which is hopefully considered for some complex mechanical problems of composites. Meanwhile, the ML method also provides accurate and efficient solution for the engineering practice.

1. Introduction

In 2016, Agrawal and Choudhary [1] proposed the four paradigms of science: empirical, theoretical, computational, and data-driven, which revealed the big potential of the data-based method for scientific problems. In recent years, machine learning (ML) has also been considered for solving mechanical problems of composite materials. It has provided new perspectives on mechanical studies using state-of-the-art computational methods [2]. For instance, Yang et al. [3] predicted stress-strain curves of binary composites; Qi et al. [4] and Golkarnarenji et al. [5] predicted elastic properties of carbon fibre based on macroscopic parameters of composites; Lucon and Donovan [6] and Yang et al. [7] calculated the macroscopic elastic properties of the composites; Gu and Chen [8] predicted composite toughness and strength; and Khan et al. [9] predicted the mechanical properties by using material type, composition and number of reinforcement and matrix layers. Convolutional neural networks (CNN) and artificial neural networks (ANN) were very common in these studies [2,6–9]. ML method is an efficient way to find out the relations between the input and output parameters, which has big potential for the studies of composite materials. For example, unidirectional fibre-reinforced laminate is one of the most widely studied composites, while the other kinds of fibre-reinforced composites, such as chopped fibre-reinforced, 2-dimensional woven fabric and 3-dimensional woven fabric, still need large amount of experiments to obtain their mechanical behaviors [10]. But the ML method may find out the mapping relations of mechanical properties between the composites with different reinforcement architectures.

Regarding non-linear regression, kernel ridge regression (KRR) is a powerful ML approach [11–16] with high accuracy and high time efficiency, but is rarely used in the published works about composite material mechanics. Nowadays, the application of ML is made simple and convenient with open-source packages, such as scikit-learn [17]. Therefore, an application of the KRR model in the nonlinear constitutive model of composite laminates is theoretically appropriate and low cost.

In this work, for the first time, the equivalent axial modulus of cross-ply composite laminates with matrix cracking is predicted using the KRR model. The data set of the ML model is established based on the published experimental data and a small number of FEA results. The optimum ML model is obtained through a series of attempts, which can be directly used to predict the axial elastic modulus degradation of $[0_m/90_n]_s$ composite laminates. The effect of data size on the accuracy is also discussed. This paper aims at translating a mechanical problem of damage into a non-linear regression problem of ML. The proposed ML model focuses on the mapping between the experimental data, instead of

* Corresponding author.
** Corresponding author.
E-mail addresses: zht@sjtu.edu.cn (H. Zhao), ja-chen@sjtu.edu.cn (J. Chen).

https://doi.org/10.1016/j.compscitech.2021.109186
Received 2 September 2021; Received in revised form 7 November 2021; Accepted 28 November 2021
Available online 29 November 2021

providing a mechanical model with idealised assumptions and simplifications. In this way, data-based methodology is hopefully considered for the composites with various reinforcement architecture, and some complex mechanical problems, such as fatigue, interface characterisation, and intralaminar fracture, etc. Meanwhile, the ML method provides an accurate and efficient solution, which is helpful in the engineering practice.

2. Data preparation

The mechanical problem of axial elastic modulus degradation in $[0_m/90_n]_s$ cross-ply laminates is illustrated and discussed in Section 2.1, where the input and output parameters are defined. m and n of the $[0_m/90_n]_s$ cross-ply laminates refer to the numbers of lamina of 0° plies and 90° plies, respectively. In Section 2.2, the published experiments and FEA results are collected and labelled to establish the data set of axial elastic modulus degradation of $[0_m/90_n]_s$ cross-ply laminates. Two testing data sets of glass-fibre-reinforced plastic (GFRP) and carbon-fibre-reinforced plastic (CFRP) are separated from the whole data set to verify prediction accuracy.

2.1. Axial elastic modulus degradation of $[0_m/90_n]_s$ composite laminates

The experimental results of composite laminates with matrix cracking [18–28] showed that the matrix crackings are usually parallel to the fibre directions and penetrate through the thickness directions in the consecutive plies with the same ply angles. They are periodically distributed in their transverse directions. Crack density ρ is defined to describe the average number of matrix crackings per length. The unit used for this is 1/mm or 1/cm. Regarding $[0_m/90_n]_s$ cross-ply laminates under uniaxial loading, matrix crackings only appear in 90° plies, while 0° plies are undamaged. Therefore, ρ refers to the crack density of 90° plies in this study. The schematic of $[0_m/90_n]_s$ laminates with matrix crackings in 90° ply are shown in Fig. 1. In Fig. 1, t_1 and t_2 refer to the thicknesses of 0° plies and 90° plies, respectively. In this paper, $t_1 = m \times t_0$ and $t_2 = 2 \times n \times t_0$, where t_0 is the ply thickness. Matrix cracking leads to the stiffness degradation of the laminated composites. This mainly concerns the degradation of axial elastic modulus $E_x(\rho)$, in-plane Poisson's ratio $\nu_{xy}(\rho)$ and in-plane shear modulus $G_{xy}(\rho)$. The degradation of axial elastic modulus is predicted using the ML method in this paper, as it is the most common used to study objects in both experiments and FEA simulations and the available data is rich. Normalised axial modulus is defined as $E_x(\rho)/E_x(0)$, where $E_x(0)$ is the axial elastic modulus of the laminate without matrix cracking. In-plane Poisson's ratio $\nu_{xy}(\rho)$ and in-plane shear modulus $G_{xy}(\rho)$ are not discussed in this paper, because the amount of available experimental data cannot meet the requirement of ML method. Theoretically, the degradation of in-plane Poisson's ratio and in-plane shear modulus can also be predicted by using the ML method, because they are also induced by the matrix cracking and local delamination, which is similar to the degradation of axial elastic modulus.

Regarding to the mechanical model, there are following idealised assumptions and simplifications of the axial elastic modulus degradation of the cross-ply composite laminates:

(1) The laminates behave as linear-elastic, orthotropic homogenized materials;
(2) The classical laminated plate theory is adopted, namely only the in-plane properties (E_x, E_y, ν_{xy} and G_{xy}) are considered;
(3) Matrix crackings are parallel to the fibre directions, penetrate through the thickness and transverse directions, and are periodically distributed in the transverse directions;
(4) Local delamination accompanying the matrxi cracking is neglected;
(5) The 0° plies of the laminates are considered undamaged.

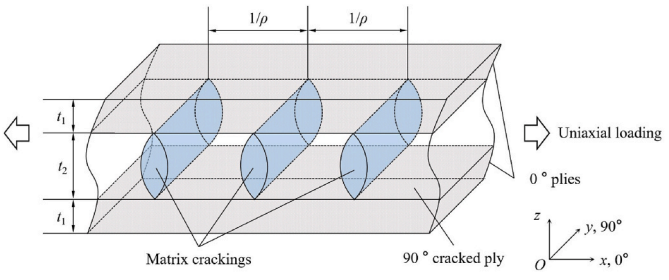

Fig. 1. Schematic $[0_m/90_n]_s$ laminate with periodic matrix crackings in 90° ply.

The mechanical assumptions and simplifications can simplify the definition and selection of the input and output parameters for the ML method. However, the process of ML is only related to the formation and accuracy of the data set, and dose not concern with the assumptions and simplifications of the mechanical model. For example, the experimental results of the axial elastic modulus degradation actually involve the effect of local delamiantion. Although the mechanical model neglects the local delamination, its influence still reflects in the experimental results of normalised axial modulus. Therefore, experimental results are proper for the establishment of ML data set, which can minimize the effect of assumptions and simplifications of the mechanical model. The ML training can also carry out based on the data set of FEA or analytical methods, but the mapping obtained by ML method in this way refers to the one of FEA or the analytical methods, instead of the mechanical problem itself.

2.2. Obtaining and labelling the data set

The purpose of this study is to predict the normalised axial modulus of the $[0_m/90_n]_s$ laminates, which is affected by the material properties of the lamina, thicknesses of the plies and crack density of 90° ply, according to the published studies regarding stiffness degradation of laminated composite with matrix crackings [20–31]. Therefore, in-plane elastic properties of the composite lamina (E_1, E_2, ν_{12}, and G_{12}), thickness of 0° ply (t_1), thickness of 90° ply (t_2) and crack density of 90° ply (ρ) are defined as input parameters, labelled as F0–F6. The normalised axial modulus of the $[0_m/90_n]_s$ laminate is defined as the output parameter, labelled as F7. The features are listed in Table 1.

The available experimental data and some of the FEA results have been collected from published works to establish the data set, as shown in Table 2. Both GFRP and CFRP laminates are involved in the data set. The total number of the samples is 467, including 380 experimental and 87 FEA results.

The purpose of this ML model is to predict the axial elastic modulus degradation of cross-ply composite laminates; therefore, a random testing data set cannot meet the requirements of the study. A GFRP laminate and a CFRP laminate are separated from the whole data set to be used as testing data. The testing data of GFRP comprises of the FEA results of a $[0_3/90_4]_s$ laminate with a layer thickness of 0.144 mm [31], labelled as Test-1. The testing data of CFRP comprises of the experiments of a $[0/90_4]_s$ laminate with a layer thickness of 0.132 mm [23], labelled as Test-2. The two testing data are chosen because their material properties, thicknesses of 0° ply and 90° ply and maximum crack densities are all within the span of the whole data set. It should be noted that the training data set does not contain its testing data.

The input data and the output data for ML training can be expressed

Table 1
Definitions of the input and output features.

	Input							Output
Label	F0	F1	F2	F3	F4	F5	F6	F7
Parameter	E_1	E_2	ν_{12}	G_{12}	t_1	t_2	ρ	$E_x(\rho)/E_x(0)$

Table 2
Laminate structures of the data set (available in supplementary data).

Reference	Stacking sequence	Ply thickness (mm)	Material	Maximum crack density (1/mm)
Highsmith (1982) [18]	$[0/90_3]_s$	0.203	GFRP ($E_1 = 41.7$ GPa, $E_2 = 13.0$ GPa, $\nu_{12} = 0.3$, $G_{12} = 3.4$ GPa)	0.708
Hashin (1986) [20]	$[0/90_4]_s$ $[0/90_6]_s$	0.147	CFRP ($E_1 = 123.0$ GPa, $E_2 = 8.7$ GPa, $\nu_{12} = 0.33$, $G_{12} = 3.9$ GPa)	0.836 0.735
Groves (1986) [21]	$[0/90]_s$ $[0_2/90_2]_s$ $[0/90_2]_s$ $[0/90_3]_s$	0.127	CFRP ($E_1 = 144.8$ GPa, $E_2 = 9.6$ GPa, $\nu_{12} = 0.31$, $G_{12} = 4.8$ GPa)	1.831 2.206 1.718 0.754
Smith (1990) [22]	$[0/90]_s$	0.155	GFRP ($E_1 = 40.0$ GPa, $E_2 = 10.0$ GPa, $\nu_{12} = 0.31$, $G_{12} = 5.0$ GPa)	2.055
Takeda (1994) [23]	$[0/90_2]_s$ $[0/90_4]_s$ $[0/90_6]_s$	0.132	CFRP ($E_1 = 148.0$ GPa, $E_2 = 9.6$ GPa, $\nu_{12} = 0.356$, $G_{12} = 4.5$ GPa)	1.324 0.925 0.657
Varna (2001) [24]	$[0_2/90_4]_s$	0.144	GFRP ($E_1 = 44.7$ GPa, $E_2 = 12.8$ GPa, $\nu_{12} = 0.297$, $G_{12} = 5.8$ GPa)	0.618
McCartney (2003) [25]	$[0_2/90_2]_s$ $[0_2/90_4]_s$ $[0_2/90_6]_s$	0.284	CFRP ($E_1 = 121.2$ GPa, $E_2 = 9.1$ GPa, $\nu_{12} = 0.32$, $G_{12} = 3.9$ GPa)	1.121 0.868 0.806
Lundmark (2005) [19]	$[0_2/90_2]_s$ $[0/90_2]_s$	0.138	GFRP ($E_1 = 44.7$ GPa, $E_2 = 12.8$ GPa, $\nu_{12} = 0.3$, $G_{12} = 3.5$ GPa)	1.222 1.260
Katerelos (2008) [26]	$[0/90]_s$	0.305	GFRP ($E_1 = 43.0$ GPa, $E_2 = 13.0$ GPa, $\nu_{12} = 0.3$, $G_{12} = 4.7$ GPa)	0.752
Loukil (2013)[a] [29]	$[0_{24}/90_8]_s$ $[0_8/90_8]_s$ $[0_2/90_8]_s$	0.5	GFRP ($E_1 = 45.0$ GPa, $E_2 = 15.0$ GPa, $\nu_{12} = 0.3$, $G_{12} = 5.0$ GPa)	0.250
	$[0_{24}/90_8]_s$ $[0_8/90_8]_s$ $[0_2/90_8]_s$		CFRP ($E_1 = 150.0$ GPa, $E_2 = 10.0$ GPa, $\nu_{12} = 0.3$, $G_{12} = 5.0$ GPa)	
Salavatian (2014) [27]	$[0/90_7]_s$	0.2875	GFRP ($E_1 = 48.1$ GPa, $E_2 = 14.2$ GPa, $\nu_{12} = 0.276$, $G_{12} = 6.7$ GPa)	2.002
Montesano (2018)[a] [30]	$[0/90]_s$	0.132	CFRP ($E_1 = 145.0$ GPa, $E_2 = 11.4$ GPa, $\nu_{12} = 0.3$, $G_{12} = 6.5$ GPa)	2.000
	$[0/90_2]_s$ $[0/90]_s$	0.5	GFRP ($E_1 = 46.0$ GPa, $E_2 = 13.0$ GPa, $\nu_{12} = 0.3$, $G_{12} = 5.0$ GPa)	
Fikry (2018) [28]	$[0_3/90_{12}]_s$ $[0_3/90_{18}]_s$	0.05	CFRP ($E_1 = 130.0$ GPa, $E_2 = 9.53$ GPa, $\nu_{12} = 0.34$, $G_{12} = 3.2$ GPa)	1.265 1.368
	$[0_3/90_6]_s$ $[0_3/90_{12}]_s$	0.1	GFRP ($E_1 = 38.2$ GPa, $E_2 = 11.1$ GPa, $\nu_{12} = 0.31$, $G_{12} = 3.9$ GPa)	0.501 0.435
Yuan (2021)[a] [31]	$[0/90_4]_s$ $[0_3/90_4]_s$ $[0_4/90_4]_s$	0.144	GFRP ($E_1 = 44.7$ GPa, $E_2 = 12.8$ GPa, $\nu_{12} = 0.297$, $G_{12} = 5.8$ GPa)	1.000

[a] FEA results.

as $\boldsymbol{X}$ and $\boldsymbol{y}$ in matrix form, as shown in Eq. (1) and Eq. (2), respectively:

$$\mathbf{X} = \begin{bmatrix} \mathbf{x}_1{}^{\mathrm{T}} \\ \mathbf{x}_2{}^{\mathrm{T}} \\ \vdots \\ \mathbf{x}_{num}{}^{\mathrm{T}} \end{bmatrix} = \begin{bmatrix} x_{11} & x_{12} & \cdots & x_{1f} \\ x_{21} & x_{22} & \cdots & x_{2f} \\ \vdots & \vdots & \ddots & \vdots \\ x_{num,1} & x_{num,2} & \cdots & x_{num,f} \end{bmatrix} \tag{1}$$

$$\mathrm{y} = \begin{bmatrix} y_1 \\ y_2 \\ \vdots \\ y_{num} \end{bmatrix} \tag{2}$$

where f is the number of input features, which equals 7 in this paper; num is the number of training data, which equals to 467 minus the number of testing data n_t; $\boldsymbol{x}_i$ is a f-dimensional vector, which refers to the feature vector of the i-th sample, and its corresponding output data is y_i; x_{ij} refers to the value of the j-th feature of the i-th sample. Every row of $\boldsymbol{X}$ refers to the input data of a single sample, namely the values of F0–F6 of this sample. The column of $\boldsymbol{X}$ refers to all input data of one of the feature. $\boldsymbol{y}$ refers to all output data, namely the values of F7.

3. ML models

Section 3.1 and Section 3.2 give brief introductions of feature selection and KRR method, respectively, and explicate the selection basis of the algorithms. Feature selection is carried out by Least Absolute Shrinkage and Selection Operator (LASSO) and cross validation (CV). Process of standardisation is illustrated in Section 3.3, which is necessary for ridge regression. Accuracy estimation methods are briefly illustrated in Section 3.4. The complete ML process for practical application is shown in Fig. 2. This paper discusses the influence of feature selection, kernel function, and data size on models' accuracy. Therefore, the process and some parameters of the ML model are different.

3.1. Process of feature selection

Features are empirically defined in Section 2.2, but the prediction model with all features may not present optimal accuracy. If some of the features are invalid for the data training or have too many outliers, removing these features can improve the accuracy of the prediction, simplify the ML model and save the cost of calculation. Therefore, feature selection is an important process before starting the ML training – especially for a problem that the ML method has not yet been applied to. The LASSO [32] and ridge regression [11] are two similar linear regression models adding L1-norm and L2-norm regularisation to the loss function of least squares method, respectively. Both the LASSO and ridge regression can calculate coefficients of the corresponding features, which can quantitatively describe the importance of the features in the

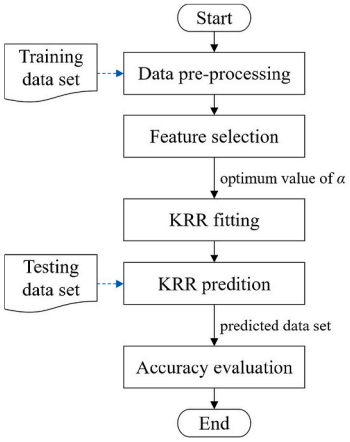

Fig. 2. Flow chart of the ML model.

regression models. However, the coefficients obtained by using the LASSO are sparse solutions, while the ones obtained by using ridge regression tend to be uniform. The sparse solutions refer to the coefficients that unimportant to the regression are zero, which make it easy to pick the unnecessary features. Therefore, the LASSO is a popular model for feature selection, which is also adopted in this paper. On the other hand, both the LASSO and ridge regression have a parameter α, which is usually obtained via trial-and-error. Therefore, CV is needed to find out the optimal model with the appropriate value of α. CV is a kind of method to evaluate the performance of ML training. In a k-fold CV process, the data set is randomly divided into k parts. Every part of the data set takes turn as testing data, while the rest of them becomes training data. Then, the ML prediction is carried out for k times, and the average score of the predictions is evaluated. Score of the ML prediction refers to the accuracy or the performance of the prediction, which can be defined as the values of average error rate, root mean squared error (RMSE) or R-squared. Three-fold CV with the LASSO is adopted in this paper, which is illustrated in Fig. 3. The available values of α are 1, 0.1, 0.01, 10^{-3}, 10^{-4} and 10^{-5}. The average scores of the LASSO CV models are obtained with different values of α, the evaluation method of which is set as the value of RMSE, namely the LASSO CV with minimum value of RMSE is provided with optimum value of α.

3.2. KRR prediction

Ridge regression is a kind of biased estimation regression method for collinear data, which is an improved least square method. For fitting ill-conditioned data, it is more practical and reliable than the least square method, as it abandons the unbiased property of the least square method and obtains the regression coefficients at the cost of losing a part of the information and reducing precision [33]. The parameter of eliminating the influence of ill-conditioned data is α, which is a coefficient of the regularisation term. α is used to control sensitivity to outliers. Therefore, the larger the α value, the less sensitivity to outliers there is. The appropriate value of α is determined by LASSO and CV in the process of feature selection.

KRR is a ridge regression method with kernel function [11]. The kernel function works by mapping data in a vector space with higher dimensionality, and considering the linear regression in such high-dimensional space. A suitable kernel function can simplify a non-linear relation in the original space as a linear relation in the high-dimensional space. The commonly used kernel functions are linear kernel, polynomial kernel, radial basis function (RBF) kernel and Laplacian kernel. The normalised axial modulus versus crack density is non-linear according to the experiments and FEA simulations. In this paper, both the polynomial kernel, RBF kernel and Laplacian kernel are adopted to predict axial elastic modulus degradation, as shown in Eqs. (3)–(5). The accuracy of the predictions using the three kernels will be compared in Section 4.3.

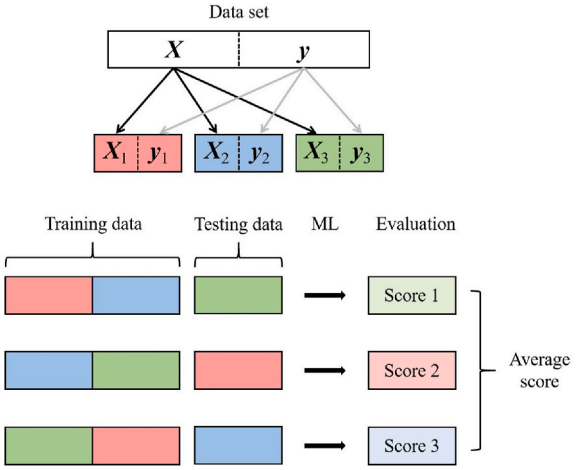

Fig. 3. Schematic three-fold CV.

Polynomial kernel:

$$K(\mathbf{x}_i, \mathbf{x}_j) = (\gamma \mathbf{x}_i{}^T \mathbf{x}_j + C)^d \tag{3}$$

RBF kernel:

$$K(\mathbf{x}_i, \mathbf{x}_j) = \exp(-\gamma \|\mathbf{x}_i - \mathbf{x}_j\|^2), \gamma > 0 \tag{4}$$

Laplacian kernel:

$$K(\mathbf{x}_i, \mathbf{x}_j) = \exp\left(-\sqrt{\frac{1}{2\gamma}}\|\mathbf{x}_i - \mathbf{x}_j\|\right), \gamma > 0 \tag{5}$$

where $K(\boldsymbol{x}_i, \boldsymbol{x}_j)$ is the kernel function; $\boldsymbol{x}_i$ and $\boldsymbol{x}_j$ are the feature vectors of the i-th sample and the j-th sample, respectively; γ is the coefficient of kernel function, which is the reciprocal of the number of features; and C and d in Eq. (3) are the constant term and polynomial degree of the polynomial kernel, where $C = 0$ and $d = 3$ in this prediction.

It should be noted that the kernel function directly defines the inner production of two samples in the high-dimensional space. The function for mapping data from the original space into the high-dimensional space is not required. Generally, in the conventional analytical closed-form solution, the normalised stiffness can be expressed as a function of orthotropic material properties, thickness of each layer, and crack density. But the KRR prediction cannot provide analytical closed-form solutions, or explain the relations between the input features (F0–F6) and the output features (F7), because the regression is obtained based on the kernel functions instead of the original data. However, the usage of kernel function simplifies the complex relation between the input and output data, and improves the performance of regression analysis. KRR prediction makes it possible to obtain the numerical solutions of complex scientific problems.

3.3. Process of standardisation

The input data for ridge regression ($\boldsymbol{X}$ in Eq. (1)) are needed to be standardised. The standardisation is carried out separately in each column. The standardised xij is defined as xij', which is obtained by Eq. (6):

$$x_{ij}{}' = \frac{x_{ij} - u_j}{s_j} \tag{6}$$

where uj is the mean value of all values of the j-th feature, which is calculated by Eq. (7); sj is the standard deviation of all values of the j-th feature, which is expressed as Eq. (8).

$$u_j = \frac{\sum_{i=1}^{num} x_{ij}}{num} \tag{7}$$

$$s_j = \sqrt{\frac{\sum_{i=1}^{num} (x_{ij} - u_j)^2}{num}} \tag{8}$$

It should be noted that the testing data are also standardised, and the parameters of standardisation (u_j and s_j) are obtained from the standardisation of input data for ML training. The mean value and standard deviation of the input data of every feature become zero and one after srandardisation, respectively. The output data for ML training $\boldsymbol{y}$ do not require standardisation.

3.4. Accuracy evaluation

Average error rate, RMSE and R-squared (R^2) are used to evaluate the accuracy of the ML. Average error rate is the average deviation of the testing data set, as shown by Eq. (9).

$$\text{Average error rate} = \frac{\sum_{i=1}^{n_t}\left(\frac{\|y_i-\widehat{y}_i\|\|}{\widehat{y}_i}\right)}{n_t} \times 100\% \tag{9}$$

where n_t is the number of testing samples; and y_i and $\widehat{y}_i$ are the true and predicted values, respectively.

RMSE in Eq. (10) is a frequently used measure of the differences between the true and predicted values. RMSE values are also adopted in the process of feature selection to determine the optimum value of α.

$$\text{RMSE} = \sqrt{\frac{\sum_{i=1}^{n_t}(y_i - \widehat{y}_i)}{n_t}} \tag{10}$$

The R-squared value is used to measure the fitness of the prediction values to the experimental values, and normally ranges from 0 to 1, as shown in Eq. (11). A model with an R^2 value over 0.9 is generally considered to be an excellent prediction.

$$R^2 = 1 - \frac{\sum_{i=1}^{n_t}\left[(y_i - \widehat{y}_i)^2\right]}{\sum_{i=1}^{n_t}\left[\left(y_i - \frac{1}{n_t}\sum_{i=1}^{n_t} y_i\right)^2\right]} \tag{11}$$

4. Results and discussions

The optimum KRR prediction model is obtained through a series of attempts. The KRR model with feature selection, polynomial kernel function ($C = 0$, $d = 3$) and an optimum value of α using the LASSO CV model ($\alpha = 0.01$ in this paper) has the minimum average error rate, the minimum RMSE, the maximum R-squared and the minimum time cost. It should be noted that the prediction models in this section all adopt the optimum parameters, except the one for comparison.

4.1. Results and discussion of feature selection

The optimum value of α is 0.01 for feature selection of the whole data set. Coefficients of the LASSO model are shown in Fig. 4. Coefficients of the LASSO model can quantitatively describe the importance of the features for the model. As shown in Fig. 4, the coefficient of F2 is zero, which indicates that F2 is useless to the training and may even decrease the accuracy of the prediction model. The accuracy of KRR prediction with F2 and without F2 will be compared in Section 4.2. F2 refers to the in-plane Poisson's ratio of the composite lamina, and the values of F2 for the whole data set are 0.316 ± 12.7%. The values of F2 not only fluctuate a little, but also may have low accuracy. The in-plane shear modulus (F3) also has low impact on the axial elastic modulus degradation. The most important feature according to feature selection is crack density (F6), which is a very reasonable conclusion. The axial and transverse moduli of the lamina, as well as the thicknesses of 0° ply and 90° ply are all essential for the axial elastic modulus degradation prediction.

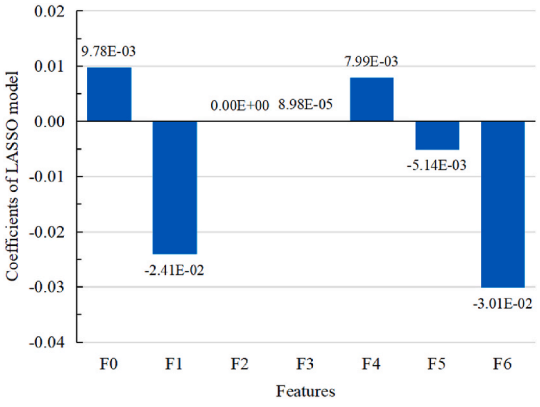

Fig. 4. Coefficients of the LASSO model.

4.2. Effect of feature selection

The accuracy of the KRR prediction with and without F2 is shown in Table 3, and the prediction results of the testing data set are plotted in Fig. 5. The optimum values of α for these models are all 0.01. Both the results of Test-1 and Test-2 show that feature selection improves the accuracy, as the average error rate, RMSE and R-squared of the KRR prediction without F2 are all better than the ones with all features. Time cost of the prediction is slightly decreased by using feature selection. Therefore, feature selection is successful in the ML method for predicting axial elastic modulus degradation.

4.3. Effect of kernel functions

Results of KRR prediction with different kernel functions are plotted in Fig. 6, and their accuracy is given in Table 4. The models with the polynomial kernel ($C = 0$ and $d = 3$) have the optimum accuracy, while the accuracies of the models with RBF and Laplacian kernels are poor. The parameter of γ in RBF kernel is also adjusted, but no KRR prediction with better accuracy was obtained. Moreover, over-fitting is present in the models with Laplacian kernel, as shown in Fig. 6.

4.4. Effect of data size

A ten-fold CV process with KRR prediction is carried out to verify the effect of data size on the KRR training accuracy. The data sizes are 10–460 with an increment of 10, and the data sets are randomly selected from Table 2. Then, 9/10 of the data are used for the KRR training and 1/10 of the data are used for KRR prediction and accuracy estimation. The accuracy of KRR prediction is evaluated by the mean values of R-squared, namely the prediction with greater mean value of R-squared is considered more accurate. Feature selection, standardisation, and polynomial kernel with $C = 0$ and $d = 3$ are adopted, which constitute the optimum process obtained in this paper. The available values of α are 1, 0.1, 0.01, 10^{-3}, 10^{-4}, 10^{-5}, 10^{-6} and 10^{-7}.

The random selection of the data sets leads to different results from a single job and another. Therefore, KRR prediction and accuracy estimation are carried out 10 times with the same data size, which are labelled as Job 1 to Job 10, respectively. The mean values of R-squared of KRR prediction with different data size are plotted in Fig. 7(a). The average R-squared values of the jobs with the same data size are plotted in Fig. 7(b). Obviously, the accuracy of the ML prediction is acceptable when the data size exceeds 400, namely the training data size exceeds 360. In Fig. 7(b), the values of R-squared are close to 0.9 with the data size greater than 400, which indicates excellent predictions. It should be noted that this accuracy estimation cannot verify the data size in need for other composite mechanical problems or other ML algorithms.

5. Concluding remarks

This study proposes an axial elastic modulus degradation prediction

Table 3
Accuracy and time cost of the KRR prediction with and without feature selection.

	Test-1		Test-2	
	without F2	with F2	without F2	with F2
Average error rate (%)	0.805	1.97	0.297	3.55
RMSE	0.0107	0.0203	0.00817	0.0337
R-squared	0.980	0.929	0.954	0.225
Prediction time (s)	0.490	0.495	0.481	0.517
Time cost improvement (%)	1.06		7.04	

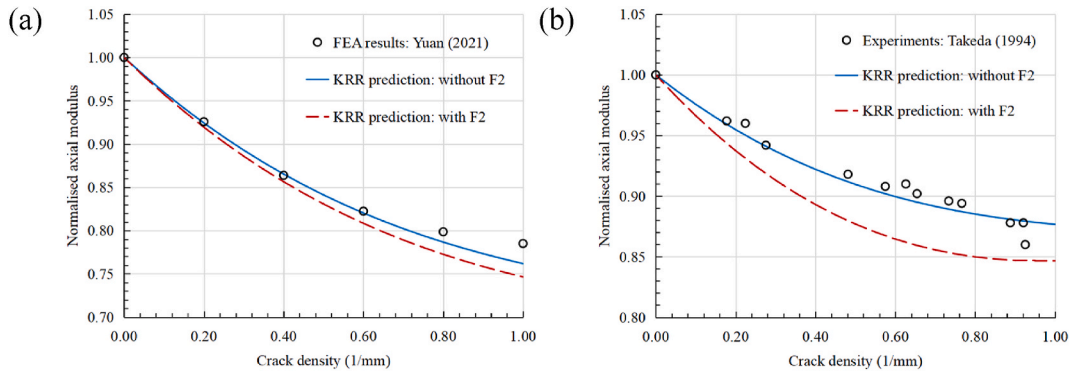

Fig. 5. Results of the KRR prediction with and without F2: (a) Test-1 ($\alpha = 0.01$); (b) Test-2 ($\alpha = 0.01$).

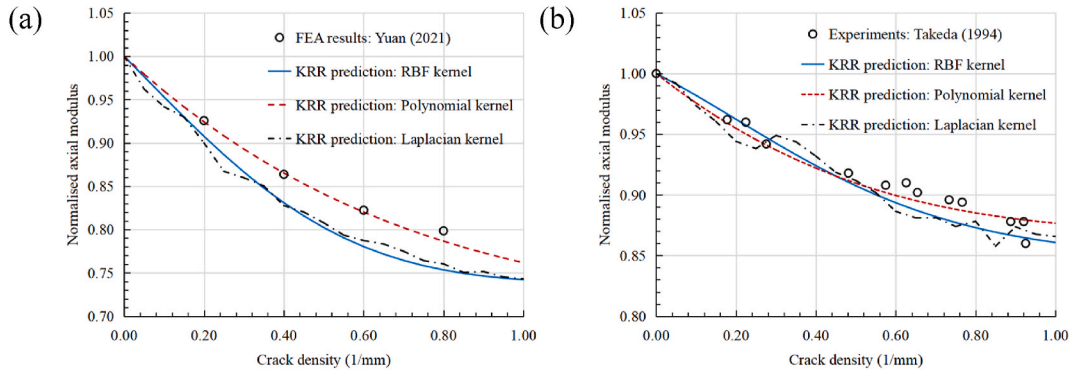

Fig. 6. Results of KRR prediction with different kernel functions: (a) Test-1 ($\alpha = 0.01$); (b) Test-2 ($\alpha = 0.01$).

Table 4
Accuracy of KRR predictions with different kernel functions.

	Test-1			Test-2		
	RBF	polynomial	Laplacian	RBF	polynomial	Laplacian
Average error rate (%)	3.85	0.805	3.72	0.887	0.297	1.24
RMSE	0.0343	0.0107	0.0327	0.0118	0.00817	0.0158
R-squared	0.796	0.980	0.815	0.905	0.954	0.830

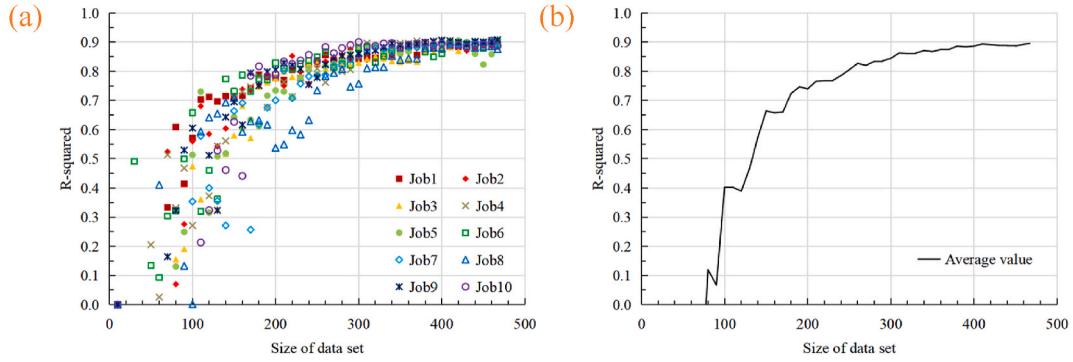

Fig. 7. R-squared of KRR prediction versus size of data set: (a) single job; (b) average valu

method of $[0_m/90_n]_s$ cross-ply laminates using ML. The data set of the ML model is established based on previously published experiments and a small amount of FEA results. Two testing data sets, GFRP and CFRP, are separated from the whole data set to verify the accuracy of the prediction from multiple indices. The optimum ML model is obtained through a series of attempts. The KRR model with standardisation, feature selection, polynomial kernel function ($C = 0$, $d = 3$) and an optimum value of α using the LASSO CV model ($\alpha = 0.01$ in this paper) is the optimum model. The prediction results of the two testing data sets have an average error rate of less than 1% and an R-squared value of greater than 0.95, which indicates very good accuracy. The effect of data size on the accuracy is discussed by using ten-fold CV with KRR model. The accuracy of the ML prediction is acceptable when the training data size exceeds 360, namely the values of R-squared are close to 0.9. The

development of this successful ML model is owed to the reliable works conducted by the mechanical researchers. However, the accuracy of ML model is dependent on the reliability and amount of the data, which may limit its application of other mechanical problems.

Regarding the axial elastic modulus degradation of $[0_m/90_n]_s$ laminates, the in-plane Poisson's ratio and in-plane shear modulus have little contribution to the degradation of axial elastic modulus. The axial elastic modulus of the lamina have positive relations with the normalised axial modulus, which indicates that the axial modulus of GFRP decreased more rapidly with crack density than the one in CFRP. In addition, the thicker 0° ply and a thinner 90° ply can both inhibit the degradation of the axial modulus of the composite laminates.

The ML method of other composite mechanical problems will be studied in the future, as it is believed that ML is promising for science and engineering. ML prediction of stiffness degradation of the laminates with arbitrarily stacking sequence will be considered in the near future. Whether the other features can improve the accuracy of ML prediction will be discussed, such as interlamina strength and fibre volume fraction.

Author statement

Mingqing Yuan: Methodology, Software, Formal analysis, Investigation, Writing - Original Draft, Visualization, Writing - Review & Editing. Haitao Zhao: Conceptualization, Methodology, Software, Data Curation, Supervision, Writing - Review & Editing. Yuehan Xie: Software, Formal analysis, Visualization. Hantao Ren: Software, Formal analysis, Visualization. Li Tian: Validation, Investigation, Resources. Zhuoxin Wang: Validation, Resources, Project administration. Boming Zhang: Software, Investigation, Project administration. Ji'an Chen: Conceptualization, Methodology, Software, Investigation, Supervision.

Declaration of competing interest

The authors declare that they have no known competing financial interests or personal relationships that could have appeared to influence the work reported in this paper.

Acknowledgement

The authors gratefully acknowledge The 3rd COMAC International Science, Technology and Innovation Week for the support of this project.

Appendix A. Supplementary data

Supplementary data to this article can be found online at https://doi.org/10.1016/j.compscitech.2021.109186.

References

[1] A. Agrawal, A. Choudhary, Perspective: materials informatics and big data: realization of the "fourth paradigm" of science in materials science, Apl. Mater. 4 (5) (2016), 053208.
[2] C.T. Chen, G.X. Gu, Machine learning for composite materials, MRS Communications 9 (2) (2019) 556–566.
[3] C. Yang, Y. Kim, S. Ryu, et al., Prediction of composite microstructure stress-strain curves using convolutional neural networks, Mater. Des. 189 (2020) 108509.
[4] Z. Qi, N. Zhang, Y. Liu, et al., Prediction of mechanical properties of carbon fiber based on cross-scale FEM and machine learning, Compos. Struct. 212 (2019) 199–206.
[5] G. Golkarnarenji, M. Naebe, K. Badii, et al., A machine learning case study with limited data for prediction of carbon fiber mechanical properties, Comput. Ind. 105 (2019) 123–132.
[6] P.A. Lucon, R.P. Donovan, An artificial neural network approach to multiphase continua constitutive modeling, Compos. B Eng. 38 (7–8) (2007) 817–823.
[7] Z. Yang, Y.C. Yabansu, R. Al-Bahrani, et al., Deep learning approaches for mining structure-property linkages in high contrast composites from simulation datasets, Comput. Mater. Sci. 151 (2018) 278–287.
[8] G.X. Gu, C.T. Chen, M.J. Buehler, De novo composite design based on machine learning algorithm, Extrem. Mech. Lett. 18 (2018) 19–28.
[9] S.M. Khan, S.A. Malik, N. Gull, et al., Fabrication and modelling of the macro-mechanical properties of cross-ply laminated fibre-reinforced polymer composites using artificial neural network, Adv. Compos. Mater. 28 (4) (2019) 409–423.
[10] V. Khatkar, B.K. Behera, Experimental investigation of composite leaf spring reinforced with various fiber architecture, Adv. Compos. Mater. 29 (2) (2020) 129–145.
[11] K.P. Murphy, Machine Learning: A Probabilistic Perspective, chapter 14.4.3, The MIT Press, 2012, pp. 492–493.
[12] N. Kim, Y.S. Jeong, M.K. Jeong, et al., Kernel ridge regression with lagged-dependent variable: applications to prediction of internal bond strength in a medium density fiberboard process, IEEE Trans. Syst. Man Cybern. C Appl. Rev. 42 (6) (2012) 1011–1020.
[13] P.Y. Wu, C.C. Fang, ChangJM, et al., Cost-effective kernel ridge regression implementation for keystroke-based active authentication system, IEEE Trans. Cybern. 47 (11) (2016) 3916–3927.
[14] Z. Guo, X. Zhao, Y. Chen, et al., Short-term passenger flow forecast of urban rail transit based on GPR and KRR, IET Intell. Transp. Syst. 13 (9) (2019) 1374–1382.
[15] M. Ali, R. Prasad, Y. Xiang, et al., Complete ensemble empirical mode decomposition hybridized with random forest and kernel ridge regression model for monthly rainfall forecasts, J. Hydrol. 584 (2020) 124647.
[16] L.H. Peng, L.Q. Zhou, X. Chen, et al., A computational study of potential miRNA-disease association inference based on ensemble learning and kernel ridge regression, Front. Bioeng. Biotechnol. 8 (2020) 40.
[17] F. Pedregosa, G. Varoquaux, A. Gramfort, et al., Scikit-learn: machine learning in Python, J. Mach. Learn. Res. 12 (2011) 2825–2830.
[18] A. Highsmith, K. Reifsnider, Stiffness reduction mechanism in composite laminates, in: Damage in Composite Materials, American Society for Testing and Materials, Philadelphia (PA), 1982, pp. 103–117. ASTM STP 775.
[19] P. Lundmark, J. Varna, Constitutive relationships for laminates with ply cracks in in-plane loading, Int. J. Damage Mech. 14 (3) (2005) 235–259.
[20] Z. Hashin, Analysis of stiffness reduction of cracked cross-ply laminates, Eng. Fract. Mech. 25 (5–6) (1986) 771–778.
[21] S.E. Groves, C.E. Harris, A.L. Highsmith, et al., An experimental and analytical treatment of matrix cracking in cross-ply laminates, Exp. Mech. 27 (1) (1987) 73–79.
[22] P.A. Smith, J.R. Wood, Poisson's ratio as a damage parameter in the static tensile loading of simple crossply laminates, Compos. Sci. Technol. 38 (1) (1990) 85–93.
[23] N. Takeda, S. Ogihara, Initiation and growth of delamination from the tips of transverse cracks in CFRP cross-ply laminates, Compos. Sci. Technol. 52 (3) (1994) 309–318.
[24] J. Varna, R. Joffe, R. Talreja, A synergistic damage-mechanics analysis of transverse cracking in [±θ/904]s laminates, Compos. Sci. Technol. 61 (5) (2001) 657–665.
[25] L.N. McCartney, Physically based damage models for laminated composites, Proc. IME J. Mater. Des. Appl. 217 (3) (2003) 163–199.
[26] D.T.G. Katerelos, M. Kashtalyan, C. Soutis, et al., Matrix cracking in polymeric composites laminates: modelling and experiments, Compos. Sci. Technol. 68 (12) (2008) 2310–2317.
[27] M. Salavatian, L.V. Smith, The effect of transverse damage on the shear response of fiber reinforced laminates, Compos. Sci. Technol. 95 (2014) 44–49.
[28] M.J.M. Fikry, S. Ogihara, V. Vinogradov, Effect of matrix cracking on mechanical properties in FRP angle-ply laminates, in: ECCM 2018—18th European Conference on Composite Materials, AML, Athens, 25–28 June 2018, pp. 793–812.
[29] M.S. Loukil, J. Varna, Z. Ayadi, Engineering expressions for thermo-elastic constants of laminates with high density of transverse cracks, Compos. Appl. Sci. Manuf. 48 (2013) 37–46.
[30] J. Montesano, B. McCleave, C.V. Singh, Prediction of ply crack evolution and stiffness degradation in multidirectional symmetric laminates under multiaxial stress states, Compos. B Eng. 133 (2018) 53–67.
[31] M. Yuan, H. Zhao, Y. Peng, et al., A micro-mechanical constitutive model for cracked plies of laminated composites considering the constraint effect of the adjacent plies, Mech. Adv. Mater. Struct. (2021) 1–12, https://doi.org/10.1080/15376494.2021.1890864 [in press].
[32] R. Tibshirani, Regression shrinkage and selection via the lasso, J. Roy. Stat. Soc. B 58 (1) (1996) 267–288.
[33] J. Tian, On SAS program of ridge regression, Appl. Stat. Manag. 3 (1999) 53–55 (in Chinese).